Elasticity and Depth Measurement using Both Secondary Speckle and Time Multiplexing Interference

Ariel Schwarz[1,2,*], Nisan Ozana[1,*], Amir Semer[1,2], Ran Califa[3], Hadar Genish[3] and Zeev Zalevsky[1]
[1]*Faculty of Engineering and the Nanotechnology Center, Bar Ilan University, Webb 1, Ramat Gan, Israel*
[2]*Department of Electrical Engineering, Jerusalem College of Engineering, Schreiboim 26, Jerusalem, Israel*
[3]*ContinUse Biometrics Ltd., HaBarzel 32b, Tel Aviv, Israel*

Keywords: Lasers, Speckle Interferometry, Scattering, Rough Surfaces, Fourier Optics and Signal Processing.

Abstract: In this paper, we describe a technique for elasticity and depth measurement via both secondary speckle and time multiplexing interference approach. Using external stimulation of elastic medium (in example: human tissue) by infra-sonic vibration, photons from different depths of the elastic medium were separated. In addition, this work uses a modulated laser that incorporates at the same scanning time, a speckle pattern tracking method for sensing surface tilting and interferometer method for sensing z-axis movements. In this paper, we present preliminary experiments showing the ability to separate data of light coming from different layers in the elastic medium.

1 INTRODUCTION

Two important parameters in characterizing elastic medium are the elasticity and depth movements of a specific point inside or on the elastic medium. These parameters divert in different medium types and can indicate mechanical and physical properties of the medium. One important medium is biological tissue characterization. Tissue mechanical property is very important since pathological and physiological characteristics are related to changes in the biomechanics of tissues. We can better understand physiological processes of tissues, diagnose and improve the treatment of various diseases by accurate measurements of tissue biomechanical changes (Greenleaf et al., 2003).

During the years, several elastography methods were proposed for different elements size. The elements imaging scales between big size (i.e. organ level methods), medium size elements (i.e tissue level methods) up to micro size elements (i.e cell level methods). Ultrasound elastography (UE) for organ level, that was first proposed in 1980, uses stimulation of a elastic medium with ultrasonic imaging (UI) technique (Dickinson et al., 1980; Sarvazyan et al., 1998). Later on based on magnetic resonance imaging (MRI) technique, magnetic resonance elastography (MRE) was presented for organ level (Muthupillai et al., 1995). The resolution of elasticity imaging by UE is of hundreds of micrometers and with MRE is of several millimeters. These two methods are limited by the spatial resolving ability of UI and MRI techniques. Another elastography method is based on atomic force microscopy (AFM) for cell level. The resolution of elasticity imaging by AFM is sub-nanometer. AFM elastography has been mainly applied for the cells than tissues due to the limited field of view and the measurement procedure (Rotsch & Radmacher, 2000). Moreover, optical imaging techniques such as multiphoton microscopy (Liang et al., 2011), confocal Brillouin microscopy (Scarcelli & Yun, 2008), laser speckle imaging (Jacques & Kirkpatrick, 1998) and optical coherence tomography (OCT) for tissue level were also developed for the elastography use.

As a further of matter, OCT in the use of Optical Coherence Elastography (OCE) is a growing field. This field of research, which began two decades ago, is today a breakthrough and rapidly developing study in medical imaging in compare to traditional methods such as cell mechanics, medical elastography, UE and

[*] *A. Schwarz and N. Ozana contributed equally to this work*

Schwarz, A., Ozana, N., Semer, A., Califa, R., Genish, H. and Zalevsky, Z.
Elasticity and Depth Measurement using Both Secondary Speckle and Time Multiplexing Interference.
DOI: 10.5220/0007521702550262
In *Proceedings of the 7th International Conference on Photonics, Optics and Laser Technology (PHOTOPTICS 2019)*, pages 255-262
ISBN: 978-989-758-364-3

MRE. Elastography using OCT was first proposed in 1998 (Schmitt, 1998) and today it is in front of optical elasticity imaging techniques. OCE focuses on the micro-scale assessment in 3D that is hard to achieve with traditional elastographic methods (Wang & Larin, 2015). There is a wide variety of methods in OCE techniques such as static/quasi-static or dynamic (continuous wave or pulsed). These methods applied to tissues either internally or externally (Sun et al., 2011).

In this paper we present detection of high frequencies vibrations using speckle and conventional interferometer. Integrating both gives the ability to detect z axes movement of a subject in addition to the tilt movement and the ability to extract data of the elastrographic different samples using modulation. The tilt extraction is done by identifiying speckle patterns trajectory using a simple correlation calculation, which enables us to detect the mechanical properties of the evaluated medium. For example: compression OCE refers to detection in a bi-layer sample; resulting in displacement versus depth due to local strain. The strain and displacement approaches are similar to the presented method. However, here the presented method is using laser as a light source with relatively high coherence length.

2 THEORETICAL BACKGROUND

2.1 Tilting and Z-axis Detection

The speckle pattern method is based upon temporal tracking of a secondary reflected speckle by imaging the speckle through properly defocused optics. The tilting changes of the object surface reflect the movement of the speckle pattern in the x-y plane (Garcia et al., 2008). The temporal tilting movement of the object surface is proportional to the change in the spatial position of the speckle pattern:

$$\beta = \frac{4\pi \tan \alpha}{\lambda} \approx \frac{4\pi\alpha}{\lambda} \quad (1)$$

Where β is the change in the speckle pattern, α is the time varying tilting angle of the object illuminated surface, λ is the illumination wavelength. By calculating the correlation, the relative movement of patterns can be extracted. This relative movement is obtained by allocating the time varying position of the correlation peak.

In order to achieve a full surface vibration data, an interferometer is used to detect the temporal changes of the surface in the z-axis. The laser source beam splits into two similar paths when only one is reflected from the vibrated object. The result is phase shifts between the two beams caused by a change in length of one of the paths. Those phase shifts create interference pattern (fringes) inside the visible speckle. The number of wavelengths contained in the path's length difference creates the fringes oscillating frequency. Using Laser Doppler Vibrometer (LDV) technique the velocity of the object surface vibration in the z-axis is measured. The z-axis vibration velocity and frequency are extracted from the Doppler shift of the reflected laser beam due to the z-axis motion of the surface. The operation of the system is described as follow (Fig. 1):

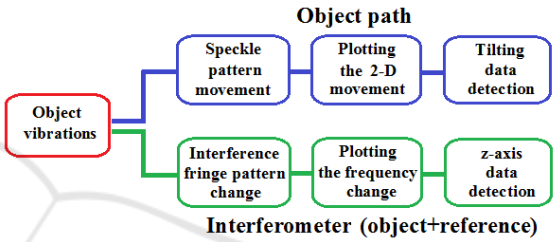

Figure 1: Flow chart of the operation system.

In order to monitor the z-axis vibration, we use the interference behaviour measurements. The constructive and destructive interferences pattern of the fringes imaging is according to the length difference ΔL between the two paths. By analysing the movement in the fringes imaging we can extract the changes in the velocity of the object's path. The number of the illumination wavelengths in the length difference (the depth of the object movement), multiple the frequency movement of the fringes pattern imaging. For example: for object movement of ΔL=1 mm with frequency of 1-2 Hz (like heart beats) and laser wavelength illumination of 532 nm, the fringes pattern movement will be with frequency of 1880-3760 Hz.

This situation of frequency multiplication leads to a problem due to camera limited frame rate. In order to solve this problem a laser modulation was used. The modulation used pulsation of the laser at frequency f_1 and modulation of the interferometer mirror at frequency of f_2 (Fig. 2).

In the regular case the speckle due to tilting is flickering at frequency of μ_1 and the fringe due to axial movement at frequency of μ_2. In our case due to the modulation at f_1 and at f_2 we obtain the following: the fringe will move at $\mu_2 + f_1 + f_2$ and the speckle at $\mu_1 + f_1$. The result is that we actually can use a low

sampling rate camera (and thus to use many pixels in space and to do large field of view analysis) since the laser will perform optical down conversion of the spectral distribution to the low band region (because it realizes optical sampling procedure) and the frequency of the mirror f_2 together with the spatial information will allow to separate between the tilting and the axial movements. Due to the pulsation of the laser we can down convert high temporal frequencies to allow their sampling with the slow rate camera. The high frequencies are folded into the low frequency spectral band sampled by the camera.

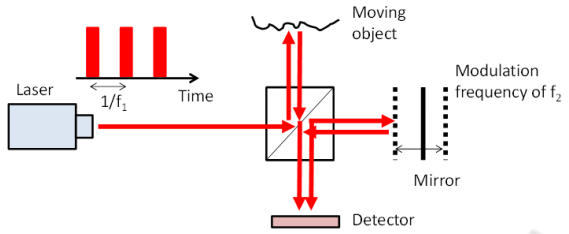

Figure 2: Schematic description of the optical system with Michelson interferometer (because of practical reasons in part of our experiments Mach–Zehnder interferometer was used).

The modulation frequency was such that the difference between it and the object frequency bandwidth is in the camera limited frame rate:

$$\cos(\lambda f_1 kt)\cos(\lambda f_2 kt) = \frac{\cos(f_1 - f_2)\lambda kt + \cos(f_1 + f_2)\lambda kt}{2} \quad (2)$$

where k is the wave number. The difference between the two frequencies (f_1-f_2) can be detected by the slow rate camera and every change in the system frequency due to the object changes can be detected.

2.2 The Elastographic Concept

Let us assume that we vibrate the medium at frequency of v_1 and that the medium has two layers. We assume that the photons coming from the inner layer have electrical field denoted by E_1 and the photons coming from the outer layer have electrical field denoted by E_2. Since the medium is soft, the different two layers (in our case it is two, but the model can be expanded to larger number of layers) are moving in a non-synchronized way: Both layers vibrate in the same frequency but there is time varying shift in their movement profile. This means that photons coming from the layer 1 and layer 2 will interfere on the camera but the interference will vary in time such that it will contribute only low DC in compare to patterns coming from photon reflecting from the same layer. We also assume that the movement amplitude is larger than the size of the scattering points in the medium. This assumption means that we assume the scattering points are moving in the medium otherwise no amplitude movement will be present. Those assumption are needed as we wish to prove that due to the lack of synchronization and since the integration period of the camera is much larger than $1/v_1$, the electrical fields E_1 and E_2 are incoherent to each other and add up in intensities and not in fields (i.e. they don't interfere with each other). This is a very important assumption because otherwise the two fields will interfere and create a new equivalent field that will generate new speckle pattern while what we aim to do is to separate between the speckle patterns generated by E_1 and E_2.

We will assume that the field E_1 generates speckle patterns having averaged speckle size of d_1 and E_2 generates speckles with average size of d_2. It is simple to design optics in which light coming from different depths create speckle patterns with different speckle dimensions. To simplify the mathematics, we will assume that the first and second speckle patterns (coming from E_1 and E_2 respectively) are modelled as follows:

$$s_1(x) = \left(2\pi {d_1}^2\right)^{-\frac{1}{2}} \sum_n e^{-\frac{(x-nd_1)^2}{2{d_1}^2}} e^{2\pi i \varphi_{1n}}$$
$$s_2(x) = \left(2\pi {d_2}^2\right)^{-\frac{1}{2}} \sum_n e^{-\frac{(x-nd_2)^2}{2{d_2}^2}} e^{2\pi i \varphi_{2n}} \quad (3)$$

Now assuming that both patterns are moving and frequency of v_1 and amplitude of $d>>d_1,d_2$ yields:

$$s_1(x - V_1 t) = \left(2\pi {d_1}^2\right)^{-\frac{1}{2}} \sum_n e^{-\frac{(x-V_1 t-nd_1)^2}{2{d_1}^2}} e^{2\pi i \varphi_{1n}}$$
$$s_2(x - V_1 t) = \left(2\pi {d_2}^2\right)^{-\frac{1}{2}} \sum_n e^{-\frac{(x-V_1 t-\delta x(t)-nd_2)^2}{2{d_2}^2}} e^{2\pi i \varphi_{2n}} \quad (4)$$

Where, $V_1=dv_1$ $\delta x \in [0,d]$. At the output plane we interfere the two fields' distributions with reference field which is moving at frequency of v_2 and add them together in the detector:

$$E_{out}(x,t) = s_1(x - V_1 t) + s_2(x - V_1 t) + r(x - V_2 t) \quad (5)$$

The reference field is a tilted planar wave with angular frequency of α and it equals to:

$$r(x - V_2 t) = e^{2\pi i \alpha (x - V_2 t)} \quad (6)$$

Where V_2 is the movement velocity of the reference beam which equals to v_2/α. The field in the previous expression is captured as intensity in the detector which also performs time integration (according to the integration time of the camera):

$$I_{out}(x) = \int |E_{out}(x,t)|^2 dt = 1 + \int |s_1(x - V_1 t)|^2 dt + \int |s_2(x - V_1 t)|^2 dt + Real\{\int s_1(x - V_1 t) s_2{}^*(x - V_1 t) dt + \int r^*(x - V_2 t)\big(s_1(x - V_1 t) + s_2(x - V_1 t)\big) dt\} \quad (7)$$

The integration time is much larger than $1/v_1$ and $1/v_2$ but smaller than $1/(v_1\text{-}v_2)$. Thus, we obtain that:

$$I_{out}(x) = 1 + c_1 + c_2 + Real\{\int r^*(x - V_2 t)\big(s_1(x - V_1 t) + s_2(x - V_1 t)\big) dt\} \quad (8)$$

Where c_1 and c_2 are space independent constants and the cross correlation expression was zero because the field distributions of the speckle patterns of s_1 and s_2 are not correlated to each other (having different dimensions and have non synchronized movement due to $\delta x(t)$):

$$\int s_1(x - V_1 t) s_2{}^*(x - V_1 t) dt = 0 \quad (9)$$

Let us now explore the expressions of $Real\{\int r^*(x - V_2 t)(s_1(x - V_1 t) dt\}$, $Real\{\int r^*(x - V_2 t)(s_2(x - V_1 t) dt\}$. To mathematically simplify we will approximate the expression of s_1 and of s_2, at least for the case of two adjacent fringes (speckles) to:

$$s_1(x - V_1 t) \approx cos^2\left(\frac{\pi}{d_1}(x - V_1 t) + \varphi_1\right) = \frac{1}{2} + \frac{1}{2} cos\left(\frac{2\pi}{d_1}(x - V_1 t) + \varphi_1\right)$$
$$s_2(x - V_1 t) \approx cos^2\left(\frac{\pi}{d_2}(x - V_1 t) + \varphi_2\right) = \frac{1}{2} + \frac{1}{2} cos\left(\frac{2\pi}{d_2}(x - V_1 t) + \varphi_2\right) \quad (10)$$

Thus, if we assume that our spatial observation point is x=0 or x-coordinate falling on the peak of one of the speckles then the expression we obtain becomes:

$$Real\{r^*(x - V_2 t)(s_1(x - V_1 t)\} \approx \frac{1}{2}\cos(2\pi\alpha V_2 t) + \frac{1}{2} cos\left(-\frac{2\pi}{d_1} V_1 t + \varphi_1\right)\cos(2\pi\alpha V_2 t)$$
$$Real\{r^*(x - V_2 t)(s_2(x - V_1 t)\} \approx \frac{1}{2}\cos(2\pi\alpha V_2 t) + \frac{1}{2} cos\left(-\frac{2\pi}{d_2} V_1 t + \varphi_2\right)\cos(2\pi\alpha V_2 t) \quad (11)$$

Thus, the final result will be:

$$Real\{\int r^*(x - V_2 t)(s_1(x - V_1 t) dt\} = \frac{1}{2}\int \cos(2\pi\alpha V_2 t) dt + \frac{1}{2}\int sin\left(-\frac{2\pi}{d_1} V_1 t + \varphi_1\right)\sin(2\pi\alpha V_2 t)\, dt + \frac{1}{2}\int cos\left(2\pi t\left(\alpha V_2 - \frac{V_1}{d_1}\right) + \varphi_1\right) dt$$
$$Real\{\int r^*(x - V_2 t)(s_2(x - V_1 t) dt\} = \frac{1}{2}\int \cos(2\pi\alpha V_2 t) dt + \frac{1}{2}\int sin\left(-\frac{2\pi}{d_2} V_1 t + \varphi_2\right)\sin(2\pi\alpha V_2 t)\, dt + \frac{1}{2}\int cos\left(2\pi t\left(\alpha V_2 - \frac{V_1}{d_2}\right) + \varphi_2\right) dt \quad (12)$$

Since the spatial periodicity α as well as $1/d_1$ are of the same order of magnitude and the time averaging integral coming due to the fact that the camera samples the output intensity at lower rate causes to the first two terms of both expression to zero (since they change at temporal frequency of αV_2 or of V_1/d_1). The third term in both expression changes (flickers) at temporal frequencies of:

$$V_{F1} = \alpha V_2 - \frac{V_1}{d_1};\ V_{F2} = \alpha V_2 - \frac{V_1}{d_2} \quad (13)$$

We can choose our parameters to make those two frequencies to be low enough so that the sampling rate of the camera will be faster than it and therefore one over the sampling rate (proportional to the integration time) will be smaller than $1/vF_1$ and $1/vF_2$ and thus the third term in both expressions will not be averaged to zero.

The main advantage of using the optical interference loop in addition to the self-interference expressed as the speckle patterns, is that it adds another parameter of V_2 allowing on one hand to average to zero the expression of $\int s_1(x\text{-}V_1 t)\, s_2{}^*(x\text{-}V_1 t) dt$=0 due to the integration time

of the camera and on the other hand not to average to zero the expression of $\int cos(2\pi t(\alpha V_1 - V_1/d_1)+\varphi_1)dt$ or of $\int cos(2\pi t(\alpha V_1 - V_1/d_2)+\varphi_2)dt$ and to allow their detection with the camera. Since each one of those two expressions flicker or temporally changes at different frequency, we can separate between them and thus to separate between s_1 and s_2, i.e. photons coming from different depths of the inspected medium. As it is detailed in Eq. 10 - 13 in comparison to OCT the depth resolution of the presented approach is based on different temporal flickering frequencies of the speckle pattern. The flickering frequency is different due to different speckle size generated by the medium elastographic properties. The depth resolution is according to Eq. 13 due to different flickering frequency.

3 EXPERIMENTAL RESULTS

3.1 Tilting and Z-axis Detection

In our setup we used the Mach–Zehnder Interferometer configuration. The vibration of the surface in the z-axis changes the path length of one of the Mach-Zender laser paths. These changes reflect in the interference pattern (fringes) of the two joined beams on a detector and camera plane.

The setup includes an illumining laser (laser diode Photop Suwtech Laser DPGL-2100F, 532 nm max 300 mW with driver Photop LDC-2500S) with a beam splitter in order to get the two paths: the object path and the reference path. The reference path consists of adjustable mirrors that can change the length of the reference path in order to calibrate the interferometer with two similar paths and according with its coherence length. Since the laser beam in the reference path gets to the detector and camera directly, while the laser beam in the object path reaches by reflection from the object, thus the intensities of the laser beams from the two paths on the detector and camera planes are not the same. For that reason, a filter was placed in the reference path to equal the two path intensities.

In order to detect only small area of the speckle pattern and the fringes pattern a pinhole of 200 µm was attached to the detector. In all our experiments a Pixelink PL-B761U camera was used as a detector. For stabilization of the fringes pattern imaging we need to correct the frequency multiplication caused by the number of wavelengths contained in the in the object path difference. The correction part of the setup consist a feedback circuit from the detector back to the reference path. The output signal from the detector was passed through an op-amp differentiator amplifier with negative feedback (Lion LE-3003D-3). The output derived signal from the amplifier derived the analogue amplifier driver (powered by a DC power supply) that control a piezo actuator (Piezomechanik SVR 1000-1) attached to a mirror in the reference path. The controlled mirror movement compensates the instability of the frequency multiplication due to the number of wavelengths in the path length changes. The object vibrations were controlled by vibration surface controller (OSC LS13C050, 2 1/4" Diameter, 50 ohm 0.5 Watt and Tektronix AFG1022 signal generator).

The described configuration includes observation of the secondary speckle pattern that is created by illuminating the object directly for tilting information and interferometer with phase shift measurements for z-axis information. In order to monitor the tilting vibration, the correlation of each of the sequential speckles images is measured. By analysing the changes in the correlation peak position, relative tilting movement of the object was extracted.

The results show that the high frequency object signal was modulated to low frequencies within the camera frame rate window according to the frequencies difference (Fig. 3).

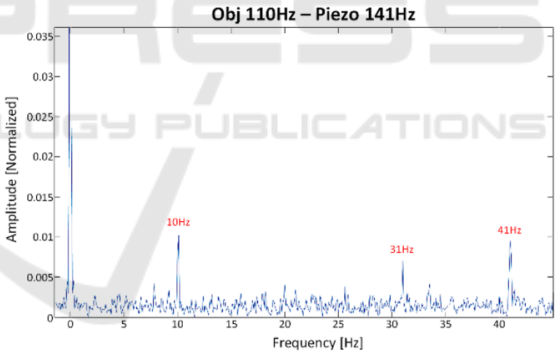

Figure 3: Piezo-mirror modulation results: the high frequency of the object was modulated by the piezo-mirror frequency to low frequencies. The difference frequency and the cut frequencies (by 100Hz of the camera) of the object and piezo-mirror.

3.2 Size of the Speckles versus Medium Depth

The first experimental validation included verification of the fact that indeed the size of the speckles change versus the depth of the medium form which they are scattered. Two experimental setups were constructed to verify this. The first in transmission (Fig. 4(a)) and the second in reflection (Fig. 4(b)).

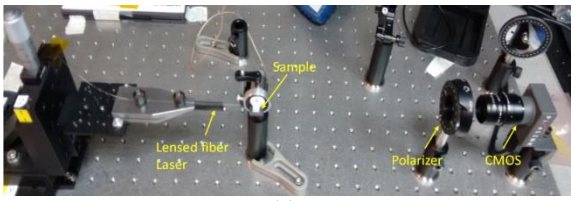

(a).

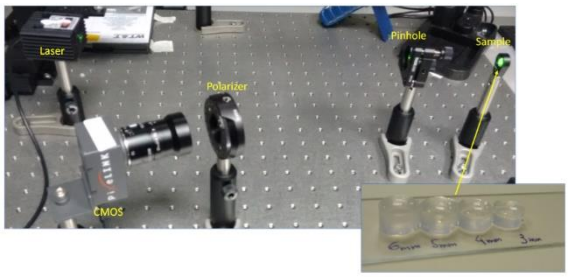

(b).

Figure 4: Experimental (a) transmission and (b) reflection setups for testing the size of speckles versus the thickness of the scattering medium.

Proper phantoms with different thicknesses were prepared as appearing in the lower right corner of Fig. 4(b). The obtained experimental results are seen in Fig. 6. In Fig. 5(a) we show the change in the speckle sizes for the transmission experiment and in Fig. 5(b) for reflection. The speckle spot diameter for different layer thicknesses are shown in Fig. 6.

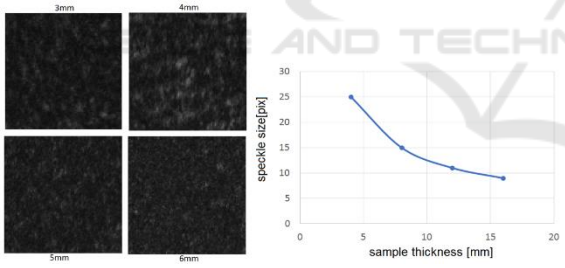

(a).

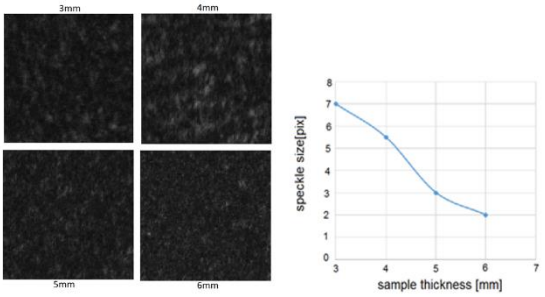

(b).

Figure 5: Experimental results (a) transmission and (b) reflection setups showing the dependence of the speckle size versus the thickness of the scattering medium.

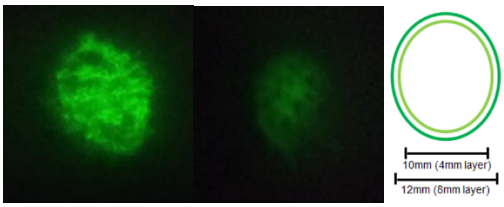

(a). (b). (c).

Figure 6: Spot diameter for different layer thicknesses: (a). Speckle spot of 8mm layer thickness (1% concentration). (b). Speckle spot of 4mm layer thickness (1% concentration). (c). Spots diameter of the two different layers thicknesses.

3.3 Coherent Temporal Elastographic Tomography

In order to validate the full proposed concept an experimental setup was established. The setup is seen in Fig.7. In this experimental setup we used a different modulation method, instead of a laser pulsation. The modulation used a controlled vibration of the object (medium layers) with piezo element at frequency f_1 and modulation of the interferometer mirror at frequency of f_2.

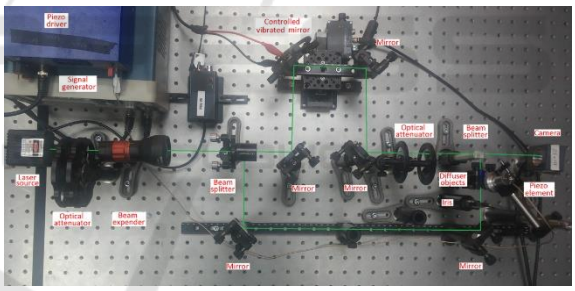

Figure 7: The experimental setup of the coherent elastographic tomography system.

The experimental results are seen in Fig. 8-9 while in Fig. 8(a) we show images of the flickering speckles and in Fig. 8(b) we show the spectrum obtained for speckles having different dimensions. In Fig. 8(c) we present the cut off frequency obtained for speckle having different dimensions (corresponding to photons coming from different depths of the inspected medium). One can see that indeed significant change in the cut off frequency of the flickering is obtained for different thicknesses of the medium and thus photons coming from different depths can be separated from each other. It is important to note that proposed concept performs the separation of the photons in the photonic level and not digitally (after performing various image processing algorithms). This separation in the photon level due

to temporal modulation and demodulation makes the proposed concept more immune to digital and electronic signal-to-noise ratio (SNR) restrictions that are very dominant in the discussed type of imaging due to the very low SNR involved.

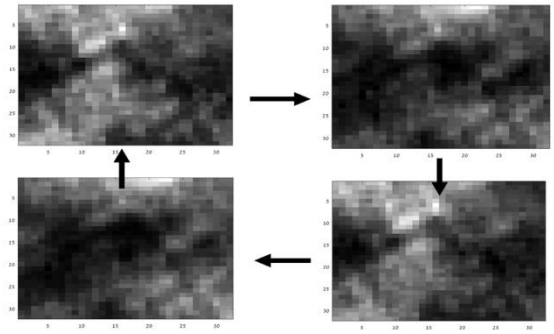

(a).

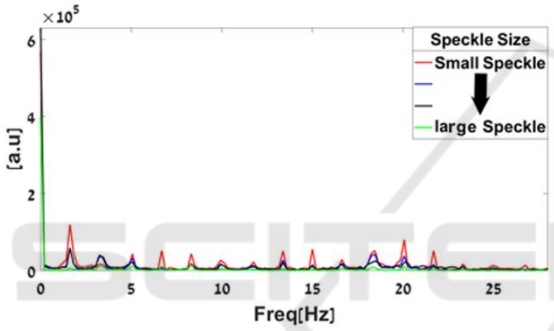

(b).

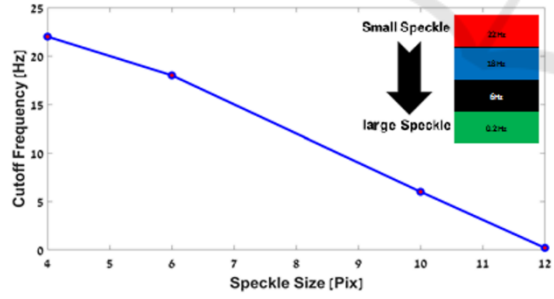

(c).

Figure 8: Experimental results for speckles flickering at different frequencies depending on the depth from which they have arrived from in the inspected medium. (a). Flickering speckles pattern. (b). Temporal spectrum of the speckle pattern with different size. (c). Cutoff frequencies for different speckle size.

The experimental average results of several experiments with 20 Hz modulations of the speckles flickering system for one and two layers and different concentrations are showed in Fig. 9. The results shown are the standard deviation of several experiments. The following experiments represents the temporal flickering of one layer, consists of 0.3% Agarose with respect to a sample with two layers one with 0.6% of agarose and the second with 0.3% of agarose. Each layer length is 4mm. The different concentrations of the agarose represent different elastographic layers. One can see that the flickering spectrum pattern is changed due to the combination between the layers. The frequency change is proportional to the elastographic value of the layer.

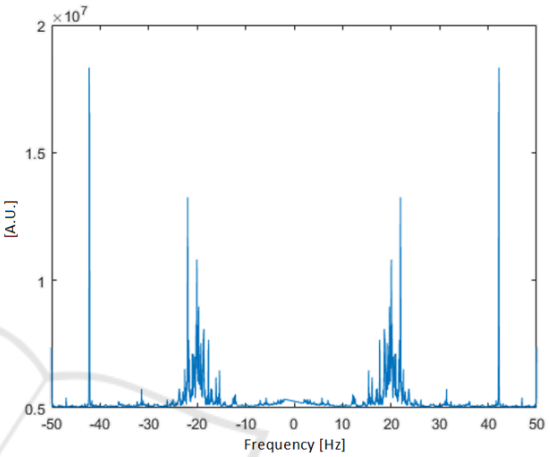

(a).

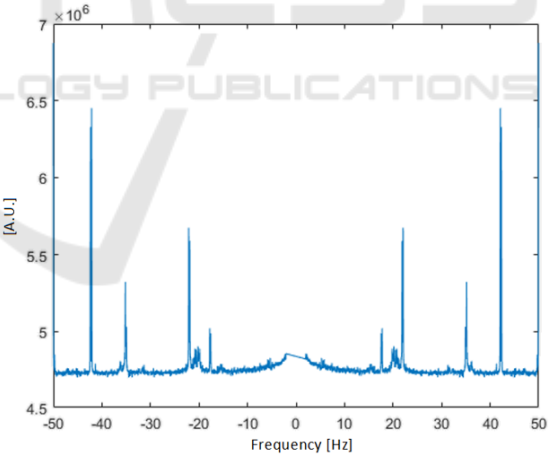

(b).

Figure 9: Experimental results of 20Hz modulations of the speckles flickering system: (a). Two layers (0.6%+0.3% concentrations, 4mm+4mm thickness). (b). One layer (0.3% concentration, 4mm thickness).

4 CONCLUSIONS

This research showed the ability to separate data of

light coming from different layers of elastic medium. In order to achieve z-axis detection (movement of the whole surface in the z direction) with tilting detection (tilting angle of the surface) Mach–Zehnder or Michelson interferometer based speckle patterns configuration can be used. In this research we showed several methods for setup modulation to down convert high temporal frequencies to allow their sampling with a slow rate camera. This research showed that different elastographic layers (that were represented by different concentrations of the agarose) changes the flickering spectrum pattern and the elastographic characters can be extracted.

REFERENCES

Greenleaf, J. F., Fatemi, M., Insana, M., 2003. Selected methods for imaging elastic properties of biological tissues. *Annual Review of Biomedical Engineering*, 5, 57-78.

Sarvazyan, A. P., Rudenko, O. V., Swanson, S. D., Fowlkes, J. B., Emelianov, S. Y., 1998. Shear wave elasticity imaging: a new ultrasonic technology of medical diagnostics. *Ultrasound in Medicine & Biology*, 24, 1419-1435.

Dickinson R. J., Hill C.R., 1980. Analysis of tissue and organ dynamics. In: Hill C. R., Alvisi C., editors. *Investigative Ultrasonology*, 1, 110–114.

Muthupillai, R., Lomas, D. J., Rossman, P. J., Greenleaf, J. F. Manduca, A., Ehman, R. L., 1995. Magnetic resonance elastography by direct visualization of propagating acoustic strain waves. *Science*, 269, 1854-1857.

Rotsch, C., Radmacher, M., 2000. Drug-induced changes of cytoskeletal structure and mechanics in fibroblasts: an atomic force microscopy study. *Biophysical Journal*, 78, 520-535.

Liang, X., Graf, B. W., Boppart, S. A., 2011. In Vivo Multiphoton Microscopy for Investigating Biomechanical Properties of Human Skin. *Cellular and Molecular Bioengineering*, 4, 231-238.

Scarcelli, G., Yun, S. H., 2008. Confocal Brillouin microscopy for three-dimensional mechanical imaging. *Nature Photonics*, 2, 39-43.

Jacques, S. L., Kirkpatrick, S. J., 1998. Acoustically modulated speckle imaging of biological tissues. *Optics Letters*, 23, 879-881.

Schmitt, J. M., 1998. OCT elastography: imaging microscopic deformation and strain of tissue. *Optics Express*, 3, 199-211.

Wang, S., Larin, K. V., 2015. Optical coherence elastography for tissue characterization: a review. *Journal of Biophotonics*, 8, 279-302.

Sun, C., Standish, B. A., Yang, V. X. D., 2011. Optical coherence elastography: current status and future applications. *Journal of Biomedical Optics*, 16, 043001.

Garcia, J., Zalevsky, Z., Garcia-Martinez, P., Ferreira, C., Teicher, M., Beiderman, Y., 2008. Three-dimensional mapping and range measurement by means of projected speckle patterns. *Applied Optics*, 47, 3032-3040.